Energy Conversion and Management 325 (2025) 119449

Contents lists available at ScienceDirect

Energy Conversion and Management

journal homepage: www.elsevier.com/locate/enconman

Enabling large-scale enhanced hydrogen production in deep underground coal gasification in the context of a hydrogen economy

Zixiang Wei [a,1], Liangliang Jiang [a,*,1], Aliakbar Hassanpouryouzband [b], Shanshan Chen [c], Yanpeng Chen [c], Yiwen Ju [d], Lele Feng [e], Kouqi Liu [f], Jiansheng Zhang [g], Zhangxin Chen [a,h,*], S.M. Farouq Ali [i]

[a] Department of Chemical and Petroleum Engineering, the University of Calgary, Calgary, AB, Canada
[b] School of Geosciences, University of Edinburgh, Grant Institute, West Main Road, Edinburgh EH9 3FE, UK
[c] Research Institute of Petroleum Exploration & Development, PetroChina, Beijing, China
[d] Key Laboratory of Computational Geodynamics, College of Earth and Planetary Sciences, University of Chinese Academy of Sciences, Beijing, China
[e] School of Safety Engineering, China University of Mining and Technology, Xuzhou, China
[f] Institute of Energy, Peking University, Beijing 100871, China
[g] Department of Energy and Power Engineering, Tsinghua University, Beijing, China
[h] Institute of Digital Twins, Eastern Institute of Technology, Ningbo 315200, China
[i] Department of Petroleum Engineering, the University of Houston, TX, United States

ARTICLE INFO

Keywords:
Hydrogen Production
Climate Change
Deep Unmineable Coals
Underground Coal Gasification
Cavity Control

ABSTRACT

Underground coal gasification (UCG) is an emerging clean energy technology with significant potential for enhanced hydrogen production, especially when coupled with water injection. Previous lab-scale studies have explored this potential, but the mechanisms driving water-assisted hydrogen enhancement in large-scale, deep UCG settings remain unclear. This study addresses this gap using numerical simulations of a large-scale deep coal model designed for hydrogen-oriented UCG. We investigated single-point and multipoint water injection strategies to optimize hydrogen production. Additionally, we developed a retractable water injection technique to ensure sustained hydrogen output and effective cavity control. Our results indicate that the water–gas shift reaction is crucial for increasing hydrogen production. Multipoint injection has been proven to be more effective than single-point injection, increasing hydrogen production by 11% with an equal amount of steam. The introduction of retractable injection allows for continuous and efficient hydrogen generation, with daily hydrogen production rates of approximately five times that of a conventional injection scheme, and an increase in cumulative hydrogen production of approximately 105% over the same time period. Importantly, the multipoint injection method also helped limit vertical cavity growth, mitigating the risk of aquifer contamination. These findings support the potential of UCG as a low-carbon energy source in the transition to a hydrogen economy.

1. Introduction

Despite the growing emphasis on renewable energy, fossil fuels continue to play a crucial role in global energy consumption, as shown in Fig. 1 [1]. Coal, a solid combustible organic rock formed by the biochemical actions of plant residues, remains a significant part of the global energy sector due to its substantial share of combined oil, gas, and coal resource [2,3]. However, it is prone to release harmful gases, including hydrogen sulfide and greenhouse gases, during gasification or combustion at the surface [4], and a large portion of coal reserves cannot be mined due to their profound depths and high water content. Therefore, rational, efficient, and clean exploitation of abundant coal resources is a key issue to be considered by developing countries, including China and India, which require large amounts of energy [5].

Underground Coal Gasification (UCG), regarded as one of the cleanest techniques for exploiting coal resources, is an idea for the in-situ conversion of coal into synthetic gas (syngas). The main components of syngas are CH_4, CO and H_2, which can be used as energy sources, as well as CO_2 and H_2S [6–8]. First proposed by the Russian

* Corresponding authors.
E-mail addresses: jial@ucalgary.ca (L. Jiang), zhachen@ualgary.ca (Z. Chen).
[1] These authors contributed to the work equally and should be regarded as co-first authors.

https://doi.org/10.1016/j.enconman.2024.119449
Received 25 September 2024; Received in revised form 12 December 2024; Accepted 23 December 2024
Available online 27 December 2024

Nomenclature

A	cross-sectional area in the flow direction, m^2
C_i	molar concentration of component i, mole/m^3
C_{si}	molar concentration of solid component i, mole/m^3
C_p	isothermal compressibility, kPa^{-1}
C_T	isobaric expansion coefficient, K^{-1}
D_{ij}	molecular diffusivity of component i in phase j, m^2/s
D_r	Initial gas molecular diffusivity at reference temperature, m^2/s
E	activation energy, kJ/mole
g	acceleration due to gravity, m/s^2
H_j	enthalpy of phase j, kJ/kg
H_{rl}	enthalpy of reaction l, kJ/kg
k_0	initial permeability, md
k	absolute permeability, md
k_j	relative permeability to phase j, dimensionless
k_{mul}	pre-defined directional multiplier factor, integer
K	thermal conductivity, J/m-day-K
n_p	total number of phases
n_b	total number of gas species in gaseous phase
n_s	total number of solid components
n_r	total number of gases involved in reactions
s_{li}	stoichiometry coefficient of component i in the reactants of reaction l
s'_{li}	stoichiometry coefficient of component i in the products of reaction l
P	fluid phase pressure, kPa
P_r	reference pressure, kPa
P_j	pressure of phase j, kPa
q_{jk}	injection/production rate of phase j in layer k, m^3/day
$q_{aq_{wk}}$	water influx rate from surrounding, m^3/day
r	reaction rate constant, day^{-1}
r_l	chemical reaction rate of reaction l, day^{-1}
R	universal gas constant, J/mole-K
S_j	saturation of phase j, fraction
t	time, day
T	temperature, K
T_r	reference temperature, K
T_j	transmissibility of phase j, m^3/s-kPa
U_j	internal energy of phase j, kJ/kg
U_s	internal energy of the solid phase, kJ/kg
U_r	internal energy of rock, kJ/kg
ν_j	fluid velocity of phase j, m/s
ν_g	gaseous phase velocity, m/s
V	grid block volume, m^3
y_{ij}	more fraction of component i in phase j, fraction
Z	elevation, m
δ_{iw}	component i concentration in aqueous phase, fraction
ϕ	pore porosity, fraction
ϕ_0	initial pore porosity, fraction
ϕ_v	current pore porosity, fraction
ϕ_f	effective fluid porosity, fraction
κ	reaction frequency factor, variable unit
ρ_j	density of phase j, kg/m^3
ρ_g	gaseous phase density, kg/m^3
ρ_{si}	density of solid component i, kg/m^3
μ_j	viscosity of phase j, cp
Φ_j	fluid potential of phase j, kPa

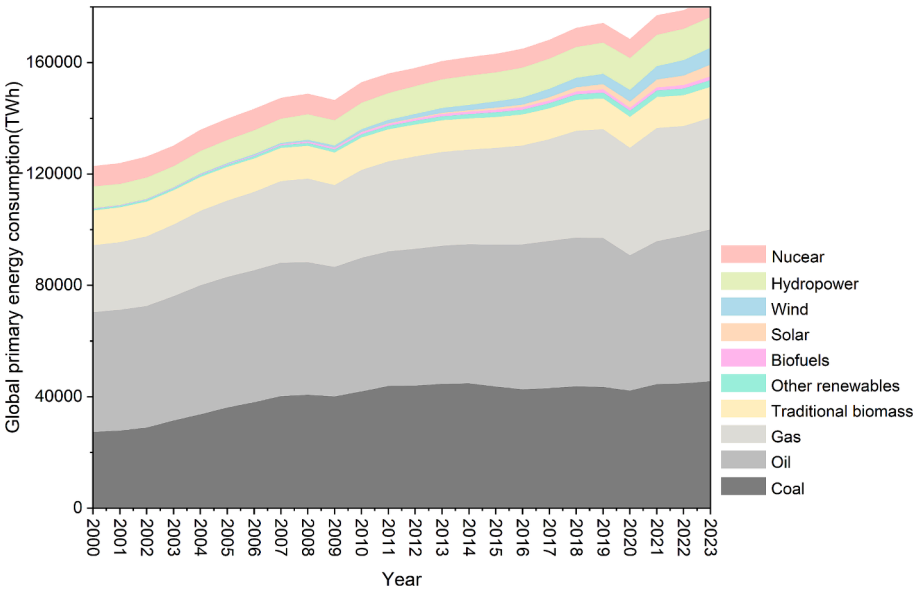

Fig. 1. Global primary energy consumption in terawatt-hours (TWh) (Redrawn from [1]).

scientist Mendeleev in 1888 [9], UCG method aims to extract energy-bearing components from coal without conventional mining. The fundamental process involves injecting oxidants such as oxygen or air into an underground coal seam through an injection well and then extracting syngas from a production well at the other end of the seam. By controlling the gas injection rate, the combustion situation in the coal seam is managed, resulting in the gasification of in-situ coal through a series of chemical reactions, including combustion, pyrolysis, and dry distillation [10–12]. Since these reactions occur underground, the UCG process offers numerous advantages over conventional gasifiers, including the prevention of harmful and greenhouse gas emissions and the reduction of labor cost [13]. Moreover, as the coal is converted to

syngas, the coal seam will form an industrial-size cavity in a post-UCG stage and several studies have demonstrated the feasibility of storing CO_2 in these cavities [14–16], thereby confirming the environmental benefits of UCG.

Hydrogen energy is anticipated to become a key clean energy source by the mid-21st century due to its high heat generation potential [17] and zero greenhouse gas emissions during combustion [18–20]. This has increased interest in UCG for hydrogen production, addressing the challenge of efficiently utilizing deep coal resources to produce clean energy [21], while ensuring low-carbon emissions and environmental protection [22]. At present, researchers in various countries have conducted studies in this field, however research gap exists, for example, large-scale enhanced hydrogen production in deep coal seams in the context of UCG.

Numerous studies have targeted Chinese coals, with notable contributions over the years. In 1995, Liang and Yu analyzed favorable conditions for hydrogen production in UCG and proposed a two-stage approach with a long tunnel and large section to enhance hydrogen yield [15]. In 2000, Yang and Yin introduced a second fire source, using dual fire sources to maintain reaction temperature, successfully verifying the concept through industrial trials [11]. Liu et al. compared a two-stage gasification technology with simultaneous oxygen-steam injection, concluding that while the former yields slightly higher hydrogen, the latter is better suited for continuous hydrogen production across various coal types, including lignite, gas-fat coal, and lean coal [23]. To further increase hydrogen production, Yang et al. recommended reverse gasification, involving the strategic withdrawal of oxidant injection wells at different timesteps to mitigate the negative impact of a diminishing reduction zone [24]. Yin et al. carried out experimental simulations on different coal types and concluded that the main source of hydrogen in pyrolysis is the dehydrogenation and condensation of fat side chains, and the amount of hydrogen production decreases with the increase of coal rank due to the higher number and types of functional groups in low-rank coals; whereas, in gasification, due to the gradual increase of char mass and carbon content with the increase of the degree of metamorphism, more reactants are able to take part in the water–gas conversion reaction, resulting in more water being reduced to hydrogen [25]. Feng et al. on the other hand focused on the effect of injected fluid conditions and found that a swirl flow injection is more favorable for hydrogen generation compared to a straight flow injection [26]. Beyond Chinese coals, Stańczyk and colleagues demonstrated that both Polish lignite and hard coal could produce hydrogen-rich syngas under various conditions of oxygen and steam [27,28]. Kapusta et al. found that high-water content in lignite could eliminate the need for artificial water supply, favoring hydrogen production from UCG [29]. The Hydrogen-oriented Underground Coal Gasification for Europe (HUGE) project highlighted that shallow coal gasification poses a high risk of gas leakage, suggesting that deep coal seams might be more suitable for the UCG process [30].

Recently, Jiang et al. provided a comprehensive review of global advancements in enhanced hydrogen production within the UCG context [8]. They concluded that, due to the prohibitively high costs of large-scale pilots, most efforts have focused on lab-scale experiments. Nevertheless, understanding the coupling of various physiochemical phenomena on a large scale and the effects of high pressure in deep coal seams remains crucial. Aiming to bridge the mentioned knowledge gap, we constructed a large-scale coal model to study enhanced hydrogen production in UCG, varying the position of a steam injection point to understand hydrogen-enhancing mechanisms in a pilot-scale setting. Moreover, we explored multipoint water injection for optimal performance. As the subsurface cavity expanded, we conceptualized a retractable water injector to maintain continuous hydrogen production. This approach, aided by a retractable steam injection, helps the underground cavity retain conformity, offering significant environmental benefits. The findings in this study provide robust support for the decarbonization of energy systems while advancing the industrial application of UCG in complex geological conditions and resource-constrained regions. They will not only contribute to reducing hydrogen production costs but also enhance the competitiveness of the hydrogen economy in the global energy transition, underscoring the pivotal role of UCG technology in achieving carbon neutrality goals. However, it has to be clarified that given the lack of pilot-scale data for comparison, a primary objective of this study is to encourage future research for a hydrogen economy in coal resource utilization.

2. Mathematical basis

In this work, the STARS module from Computer Modeling Group (CMG) Ltd. was used for modelling study. Originally developed to simulate reservoirs with complex thermal and chemical processes, STARS was applied by Seifi et al. to combustion tube experiments, pyrolysis, and self-gasification [31]. They proposed that this porous medium simulator could analogize the UCG process to thermal recovery by treating the residual ash as a rock structure, the coal's water content as initial water saturation, and the combustible material as a heavy oil component in the UCG process and hydrogen reservoirs, respectively. The simulation results showed good agreement with experimental outcomes and analytical methods, confirming the feasibility of this numerical simulation approach. Moreover, other studies have also demonstrated the utility of applying this numerical method to conduct relevant researches [32–35]. In this section, the mathematical equations for mass, momentum, and energy conservation laws in the STARS module will be described.

2.1. Governing equations

In porous media, fluid transport conforms to Darcy's law, which describes the momentum conservation of fluids with the following mathematical form [36]:

$$v_j = -\frac{kk_j}{\mu_j}\nabla\Phi_j \tag{1}$$

Detailed explanations of the variables in this section are provided in the following and the Nomenclature section. The conservation equation of mass with the consideration of a grid volume V is given by [37]:

$$\sum_{j=1}^{n_p}\phi D_{ij}\rho_j\Delta y_{ij} + \sum_{j=1}^{n_p}T_j\rho_j y_{ij}\Delta\Phi_j + V\sum_{l=1}^{n_r}\left(s'_{li}-s_{li}\right)r_l + \sum_{j=1}^{n_p}\rho_j q_j y_{ij} + \delta_{iw}\rho_w q_{aq_w} = \left(\frac{V}{\Delta t}\right)\left(\left(\phi_f\sum_{j=1}^{n_p}\rho_j S_j y_{ij}\right)^{n+1} - \left(\phi_f\sum_{j=1}^{n_p}\rho_j S_j y_{ij}\right)^{n}\right) \tag{2}$$

The first term on the left-hand side of equation presents the diffusion of mass, where D_{ij}, the sum of molecular diffusivity and the diffusivity arising from convection processes, was proposed by Perkins [38] to address the challenge of modeling the double-diffusive natural convection phenomenon in a cavity. This phenomenon encompasses the thermal effects on diffusions caused by temperature gradients and the substantial effects induced by concentration gradients in chemical reactions [38–41]. The Stokes-Einstein theory of effective molecular diffusion is assumed to be applicable due to the non-isothermal nature of the UCG process [42]. Due to the data limitations, this study assumes that effective molecular diffusion coefficients are approximately equal for all gas components, with the empirical exponent n taking the value 1:

$$D_{ij} = D_r\left(\frac{T}{T_r}\right)^n \tag{3}$$

The second term on the left in equation describes the mass convection, while Tj implies the phase permeability as:

Table 1
The effective kinetics of various reactions considered in UCG [36].

Chemical reactions	Reaction formula	Enthalpy	k_{l0}	E_l
Coal Pyrolysis	Coal → Char + CO_2 + CO + H_2 + CH_4 + Ash	0	1.44E10	150
Char Oxidation	C + O_2 → CO_2	−393	9.00E10	100
Boudouard	C + CO_2 → 2CO	+172	3.20E10	249
Steam gasification	C + H_2O → H_2 + CO	+131	4.70E10	156
Methanation	C + 2H_2 → CH_4	−75	1.50E10	200
Water-gas shift	CO + H_2O ↔ CO_2 + H_2	±41	2.40E08	12.6
Steam-methane reforming	CH_4 + H_2O ↔ CO + 3H_2	±206	2.70E07	236

$$T_j = \left(\frac{A}{\Delta l}\right)\left(\frac{kk_j}{\mu_j}\right) \quad j = 1, \cdots, n_p \tag{4}$$

The solid phase in the model is expected to undergo significant alteration due to a series of chemical reactions, including thermal pyrolysis of coal and combustion reactions involving char. Therefore, the third term on the left-hand side of equation accounts for the conservation of solid component i and may be mathematically expressed as:

$$V\sum_{l=1}^{n_r}(s'_{li} - s_{li})r_l = (\frac{V}{\Delta t})((\phi_v C_i)^{n+1} - (\phi_v C_i)^n) \tag{5}$$

where ϕ_v indicates porosity that is affected by changes in temperature and pressure under non-isothermal conditions, following this relationship:

$$\phi_v = \phi_0\left(1 + C_P(P - P_{ref}) - C_T(T - T_{ref})\right) \tag{6}$$

Additionally, the void space within UCG is anticipated to change due to reactions such as thermal pyrolysis of coal and ash generation. Consequently, it is imperative to calculate the fluid volume fraction in accordance with the following equation:

$$\phi_f = \phi_v\left(1 - \sum_{i=1}^{n_s}\frac{C_{si}}{\rho_{si}}\right) \tag{7}$$

The conservation of the energy equation is presented in equation. First two terms on the left-hand side of it delineate heat convection and heat conduction respectively, while the following two terms denote the heat generated from chemical reactions and the outside heat input:

$$\sum_{l=1}^{n_b}\sum_{j=1}^{n_p} T_j\rho_j H_j\Delta\Phi_j + \sum_{l=1}^{n_b} K\Delta T + V\sum_{l=1}^{n_r} H_{rl}r_l + \sum_{j=1}^{n_p}\rho_j H_j q_j = \left(\frac{V}{\Delta t}\right)(\xi^{n+1} - \xi^n) \tag{8}$$

The right-hand side of equation refers to the energy accumulation and to calculate the internal energy ξ, we take a weighted average of energy values from all phases.

$$\xi = \phi_f\sum_{j=1}^{n_p}\rho_j S_j U_j + \phi_v C_s U_s + (1 - \phi_v)U_r \tag{9}$$

For simplicity, permeability is expressed in terms of porosity, as demonstrated by equation in our study. The pre-defined directional multiplier factor k_{mul} has been set to 14, which is indicative of the anisotropic characteristics of coal, thereby reflecting the influence of complex cleats in mass transfer [5].

$$k = k_0\exp\left[k_{mul}\left(\frac{\phi - \phi_0}{1 - \phi_0}\right)\right] \tag{10}$$

2.2. Primary reactions

Since the gaseous components account for the majority of the reactants and products in the chemical reactions during UCG process, the current study employs a model that considers seven distinct gas components, including steam, hydrogen, nitrogen, oxygen, carbon dioxide, carbon monoxide, and methane. In terms of solid components, the formation of charcoal and residue (ash) during the pyrolysis of in-situ coal will be included. Thus, the total number of components considered in this model is ten.

As listed in Table 1, a total of nine chemical reactions are computed in our model, encompassing both homogeneous and inhomogeneous reactions. Notably, the last two reactions, i.e., the water–gas shift and steam-methane reforming, are modelled as two-way reactions. The reaction rate is simulated using Arrhenius reaction kinetics, expressed as below:

$$r_l = k_l\prod_{i=1}^{n_c} C_i = k_{l0}\exp(-E_l/R\overline{T})\prod_{i=1}^{n_c} C_i \tag{11}$$

3. Model conceptualization

Fig. 2 illustrates an emerging technique for developing UCG that is better suited to deep unmined coal seams, proposed by Jiang et al. [43].

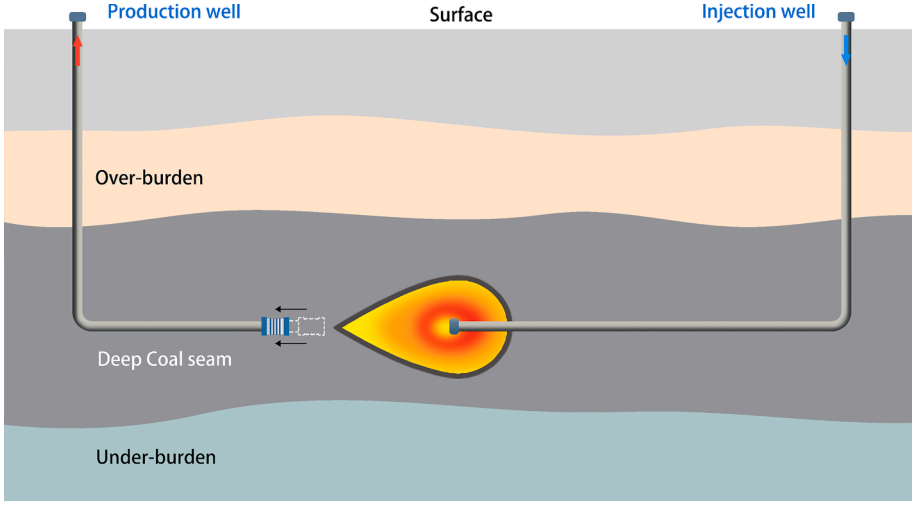

Fig. 2. Cross-sectional view of the retractable production well method (Redrawn from [43]).

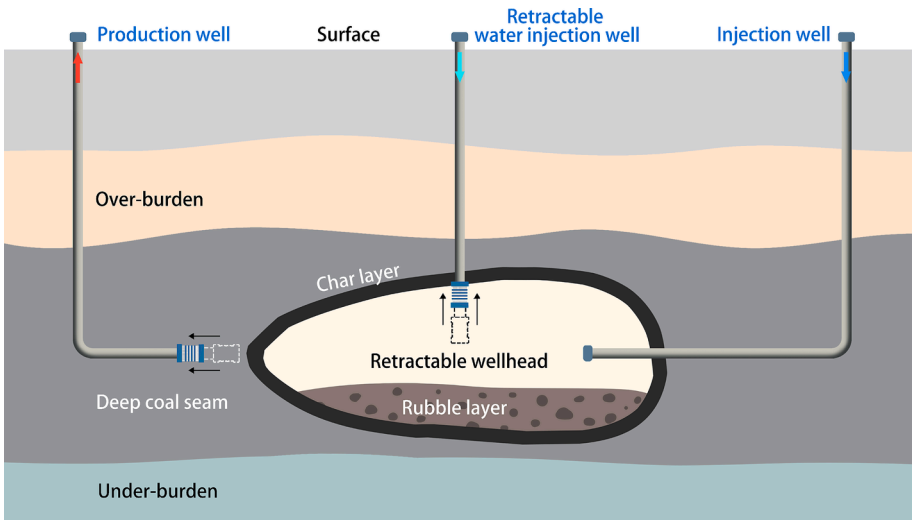

Fig. 3. Sketch of retractable water injector for enhanced hydrogen production.

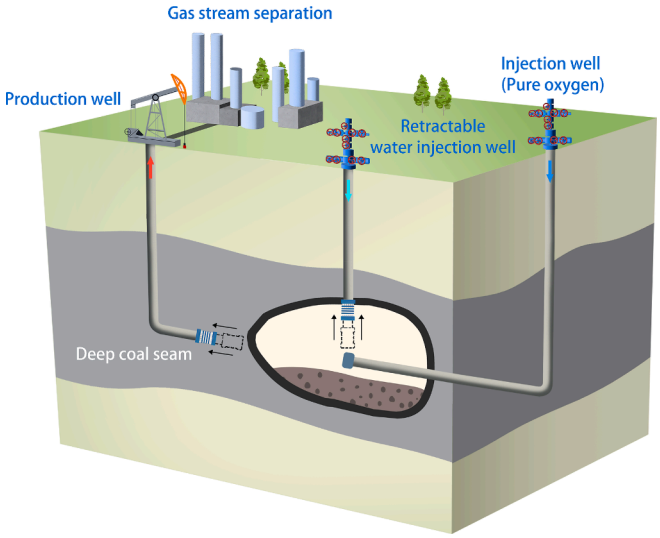

Fig. 4. Three-dimensional view of constructed model with retractable water injection well.

Table 2
Parameters of Santanghu Basin coal sample for model initialization [43].

Properties	Value	Unit
Coal thickness	25	m
Initial average pressure	7,570.5	kPa
Initial temperature	40.5	℃
Porosity	0.66340	fraction
Permeability (i/j/k)	2/2/2/	md
Water saturation	0.7	fraction
Coal density	1,300	kg/m^3
Char density	1,740	kg/m^3
Ash density	2,500	kg/m^3
Coal concentration	75,900	$gmol/m^3$
Thermal conductivity of rock	200,000	J/m-day-°C
Thermal conductivity of solid	30,240	J/m-day-°C
Thermal conductivity of water	48,384	J/m-day-°C
Thermal conductivity of gas	4,000	J/m-day-°C
Thermal capacity coefficient of solid	14.78	J/gmol-°C
Thermal expansivity of coal	33 x 10^{-6}	1/°C
Compressibility of coal	3.0 x 10^{-7}	1/kpa
Initial gas diffusion coefficient	0.05184	m^2 /day
Injected water temperature	205	℃
Steam quality	0.75	fraction

It involves withdrawing a production well at appropriate times to sustain an interwell communication while preventing a premature production of oxidant. This work aims to promote hydrogen production in UCG in deep coal seams, and thus the idea of a retractable producer was utilized.

Based on the model presented in Fig. 2, a third well for water injection was erected as shown in Fig. 3. Ideally the erection of the water injector happens when a good UCG cavity is developed in order not to quench the ignition process. In addition, in analogy to the retractable production well, the water injection well features a retractable end such that the water injection points boast the capability to move in accordance with the growth of the cavity.

Fig. 4 depicts the constructed 3D model based on the sketch. Aiming to explore the impact of water injection on hydrogen production through numerical simulations, the model comprises 240,950 grid blocks (79 × 61 × 50) with a grid width of 0.5 m. To bear practical applicability of the simulation results, the physical properties of deep coal in the Santanghu Basin, Xinjiang, China were adopted. No-flow boundary conditions were considered. The parameters associated with the initialization of the system are listed in Table 2. In this study pure oxygen was injected.

4. Results and analysis

The model involved applying a heater at the toe of the oxidant

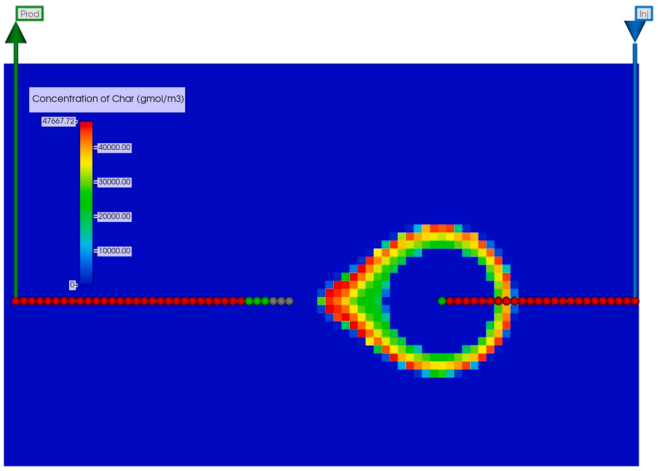

Fig. 5. Distribution of char on 30th day in no-water injection base model.

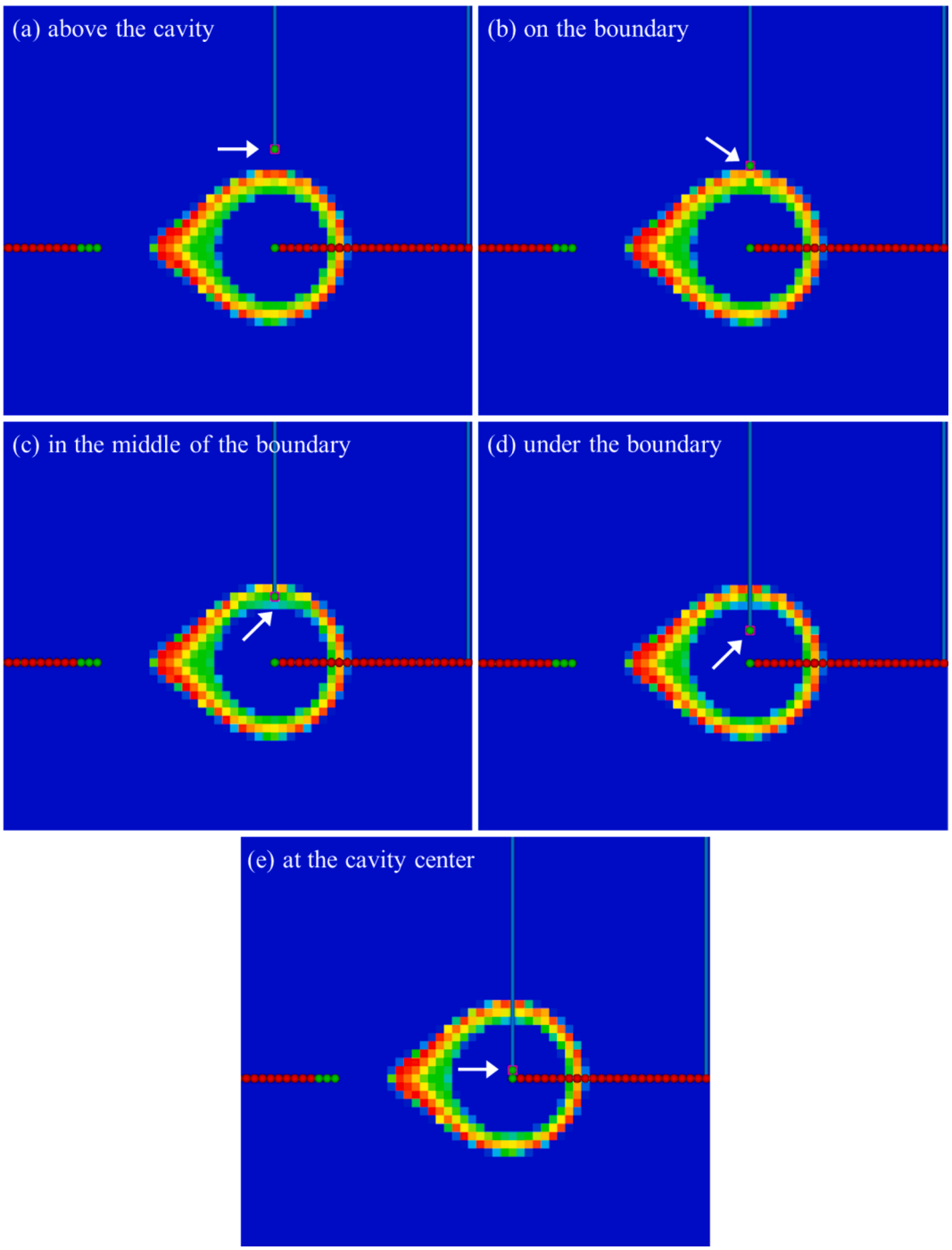

Fig. 6. Different scenarios of single-piont water injection.

injection well for two days to simulate the ignition process. From day 3, pure oxygen was continuously injected into the coal seam, with the supply rate gradually increasing over time to account for an expanding subsurface cavity. It is widely accepted that to produce H_2 on an industrial scale through underground coal gasification (UCG), external water is necessary to provide the required amount of elemental hydrogen. Consequently, the adoption of a water injection well is generally the preferred method for increasing hydrogen production in coal mines without a nearby aquifer. However, few studies have explored the mechanisms underpinning an enhanced hydrogen production in the context of UCG, especially on a large-scale. This research gap galvanizes the modelling study in this paper to determine the optimal method of enhancing hydrogen production under various water injection scenarios. Additionally, this section discusses the feasibility of controlling the multidirectional cavity's growth in the vertical direction by maneuvering the water injection well. To facilitate a comparison, a base model without water injection was constructed. Fig. 5 depicts the cavity growth on day 30 in a cross-sectional view for the base model. The primary reaction underlying the UCG process is the pyrolysis of coal to char, ash, and volatile gases. Therefore, the char concentration serves as a good reference to approximate the boundary of the cavity, as revealed in Fig. 5. It is to note that the blue region within the colored belt denotes the void wherein all char has been consumed in its entirety, whereas the outside blue area signifies intact coal seams.

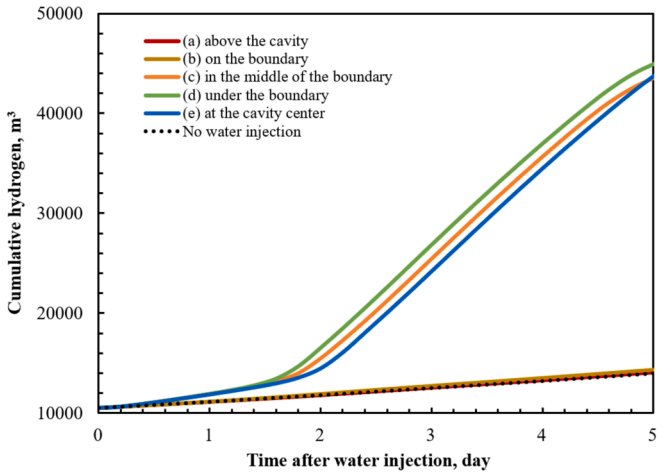

Fig. 7. Cumulative hydrogen production after water injection.

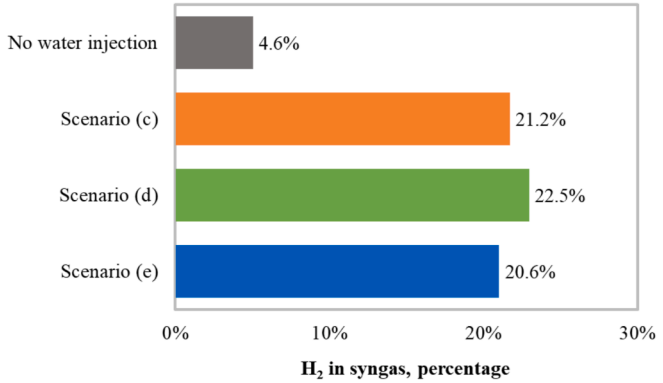

Fig. 8. Average hydrogen fraction in syngas within the observation period.

4.1. Hydrogen enhancing mechanisms

4.1.1. Single-point injection

Perforation is a crucial process that enables fluid flow between a wellbore and a formation. In UCG, a cavity with its boundary is revealed to feature various chemical regions, e.g., coal pyrolysis, combustion, gasification and dehydration [35]. In order to assess the most favorable regions to hydrogen content in the syngas, single perforation was investigated in the very first step. Five different scenarios of single perforation were considered, as illustrated in Fig. 6: (a) above the cavity; (b) on the boundary; (c) in the middle of the boundary; (d) under the boundary; (e) at the cavity center. To ensure consistency, all models were subject to the same water injection.

As the underground cavity grows, over time a dynamic, moving boundary leads to the stationary water injection point traversing from one region to another. To minimize this impact, an observation window of 5 days following the water injection was selected for the comparison. Fig. 7 displays the results of cumulative hydrogen production in various single-point injection scenarios. It shows that water injection above or on the boundary, i.e. the (a) and (b) scenarios, contributed to a negligible hydrogen increment as the curves virtually overlap that of the no water injection base case. In contrast, in the other three scenarios, although hydrogen production did not exhibit a dramatic increase during the preceding day and a half, it still experienced a significant overall rise during the same period. This may be attributed to the introduction of injected water, which initially reduced the temperature required for the reduction reaction converting steam into hydrogen, as the injected fluid temperature was substantially lower than the ambient temperature within the cavity. However, there was a delayed but

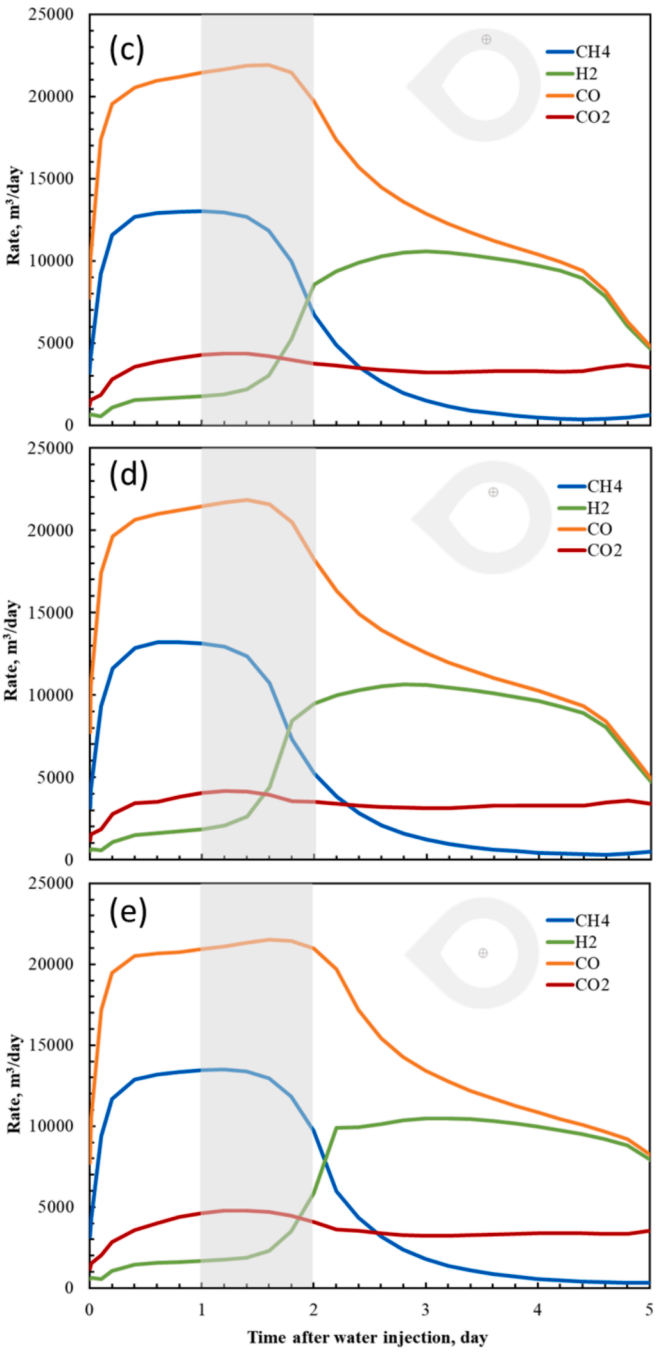

Fig. 9. Gas rate of the three hydrogen-enhanced scenarios (c), (d) and (e).

notable increase in hydrogen production as exothermic reactions continued due to the sustained injection of oxidants. Notably, scenario (d), involving water injection below the cavity boundary, demonstrated the greatest potential for enhancing hydrogen content. Furthermore, the total hydrogen production in scenario (c) surpassed that of scenario (e) until the conclusion of the observation period.

The hydrogen production results of the three effective injection scenarios are quantitatively presented in Fig. 8 in the form of an observation-averaged fraction of hydrogen in the cumulative syngas. This modelling outcome in Fig. 8 reveals that, in comparison to the base model, water injection at a suitable location within the UCG cavity boasts a potential to increase H_2 content by nearly 5 times. This change is in general agreement with the two-stage gasification for hydrogen production study by Liu et al. In that study the volume of hydrogen

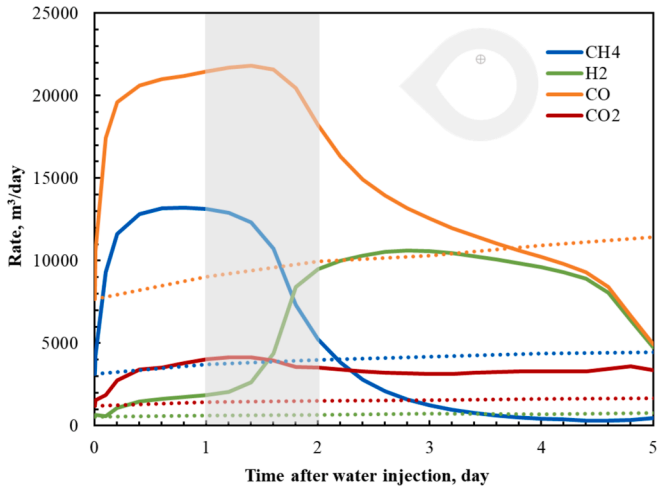

Fig. 10. Gas rate comparison between scenario (d) and the base model (dashed lines).

accounted for 10.63 % of the syngas at the stage of gasification with the injection of 80 % oxygen, whereas after the subsequent gasification with the injection of water vapour, the percentage of hydrogen rose to 42.20 %, which is four times of the original ratio [44]. However, it is important to note that the water injection derived hydrogen boosting potential heavily hinges on a number of factors, e.g., coal properties, formation water content, process setting, and surrounding water intrusion. Therefore, this paper intends to reveal the physiochemical drivers to enhanced hydrogen production with external water injection, and, therefore, it is out of the scope of this work to maximize the syngas output of a particular coal seam.

The abovementioned analysis concludes that water injection underneath the char boundary (scenario (d)) favours most the H_2 generation in the tested schemes. In-depth analysis was followed to probe the mechanisms leading to additional hydrogen content. In Fig. 9, the gas rates of CH_4, H_2, CO and CO_2 of the three hydrogen-contributable cases were compiled and compared. In general, a rate variation of each gas exhibited a very similar trend among the three scenarios. For example, the rates of CH_4 and CO rose steeply upon water injection until reaching a relatively stable high rate in less than half day, followed by a sharp decline in 1–2 days. The H_2 rate underwent a slow increase, followed by a sharp boost in about 1.5 days after water injection until it entered an approximate plateau of 10,000 m^3/day or so. In all cases hydrogen production started to decline at the end of the observation time, indicating that the relative position of the injection point to the newly expanded boundary turned unfavorable to hydrogen production. The rate of CO_2 did not change significantly throughout the examined period in all hydrogen-enhanced cases. The grey-out region in Fig. 9 marked the drastic changes in a gas rate, wherein some minor differences are discernable. A sharp boost in H_2 occurred first in (d), i.e., injection beneath the char boundary, followed by (c) and (e). Furthermore, in conjunction with variations in hydrogen production as shown in the curves, the CO and CH_4 rates exhibited an opposite change; e.g., (e) features the longest duration of the high-rate plateau, followed by (c) and (d).

To further unveil the reactions leading to hydrogen production under water injection, gas rates were compared between scenario (d) and the no-water injection base case in Fig. 10. In the base case, the gas rate was relatively steadied during the short observation time window except for CO, which showed a constant rise. The plots of scenario (d) imply that the intervention of external water triggered a rate boost for all gases in the beginning, with prominent increments to CH_4 and CO. The notable reactions involving water are steam gasification, a reversible water–gas shift and steam-methane reforming (see Table 1). Therefore, an abrupt abundance in water initially drives these reactions for more CO and CO_2. However, in comparison to CH_4 and CO, the disproportionately slow increments in H_2 and CO_2 may indicate active reactions of Boudouard and methanation which help consume H_2 and CO_2 for more CH_4 and CO.

The effects of injected water on a gas rate reversed 1 day later as the abundance of water was vanishing; i.e., H_2 gained incremental momentum whilst the rates of CH_4 and CO began plummeting as demonstrated in Fig. 10. This drastic change in the pattern of a gas rate is reflective of the engaging chemical reactions. For example, the rate of CH_4 that plunged to almost none at the end of the observation time means that the methanation process was either feeble or overwhelmed by a steam-methane reforming reaction. In addition, a soaring H_2 rate and a diving CO rate may imply a prevailing water–gas shift process in which CO was converted into H_2. Furthermore, the reactions of steam gasification and steam-methane reforming may be active in generating H_2 and CO, and the produced CO will be predominantly reduced in the subsequent water–gas shift event. Therefore, while it is unreasonable to rule out the contribution of other reactions, one can conclude that the water–gas shift phenomenon contributed substantially to the enhanced hydrogen production.

Fig. 11 shows the temperature value of each injection point before water was injected. The relative low temperature above the cavity and on the outer boundary reinforced the results that these two injection positions unfavoured hydrogen-oriented endothermic gasification reactions. On the contrary, the other three injection scenarios were based on elevated-temperature locations, with scenario (d) had the highest temperature of 1004 °C as it situated within the combustion region as supported in Fig. 11. Counterintuitively, the higher-temperature scenario (c), i.e., 885 °C, was slightly outperformed by the 752 °C scenario (c) in hydrogen production. This underperformance was likely due to limitations in mass transport because the char boundary was less permeable than the void. Therefore, the injection point under the boundary resulted in the best performance of hydrogen production for two main reasons. First, the very high temperature in the combustion zone favours endothermic gasification reactions. In addition, the proximity to both the char layer and the void space where the reactive gases are abundant is beneficial to the reactions.

The introduction of external water exerts a strong impact on cavity temperature. Before water injection the cavity had an active combustion ring with temperature as high as over 1000 °C as shown in Fig. 11. However, at the end of the observation period the prevailing temperature in the cavity was about 400 °C, with the peak at about 500 °C on the thin combustion ring (see Fig. 12). This striking disparity is attributable to the cooling effects of water and the promoted endothermic gasification reactions. It is worth noting that an elevated temperature is one of many indicators of a sustainable UCG cavity which grows and evolves to generate sizable syngas. Thus, the design of a water injection rate must be carefully justified on a case specific basis.

4.1.2. *Multipoint injection*

In field operations, wellbores are commonly utilized in the form of multiple perforations as opposed to single perforation, as the latter may incur higher maintenance costs due to the risk of clogging. The use of multiple perforations in the present study aims for increased hydrogen production. It is important to note that determining the optimal number of perforations is not the objective of this subsection. Instead, the focus is on whether multipoint water injection exhibits superior hydrogen production capabilities compared to the single-point scenario.

To facilitate a comparison, the single-point analysis will be extended to multipoint scenarios. However, multiple perforations require occupying more grids. Therefore, to avoid an overlap between cases, only three scenarios were considered: (a) above the boundary; (b) under the boundary; and (c) in the cavity. The number of perforations is three, and the locations in each scenario are illustrated in Fig. 13.

Fig. 14 depicts the cumulative hydrogen production of all multipoint injection scenarios for the same 5-day observation window, with

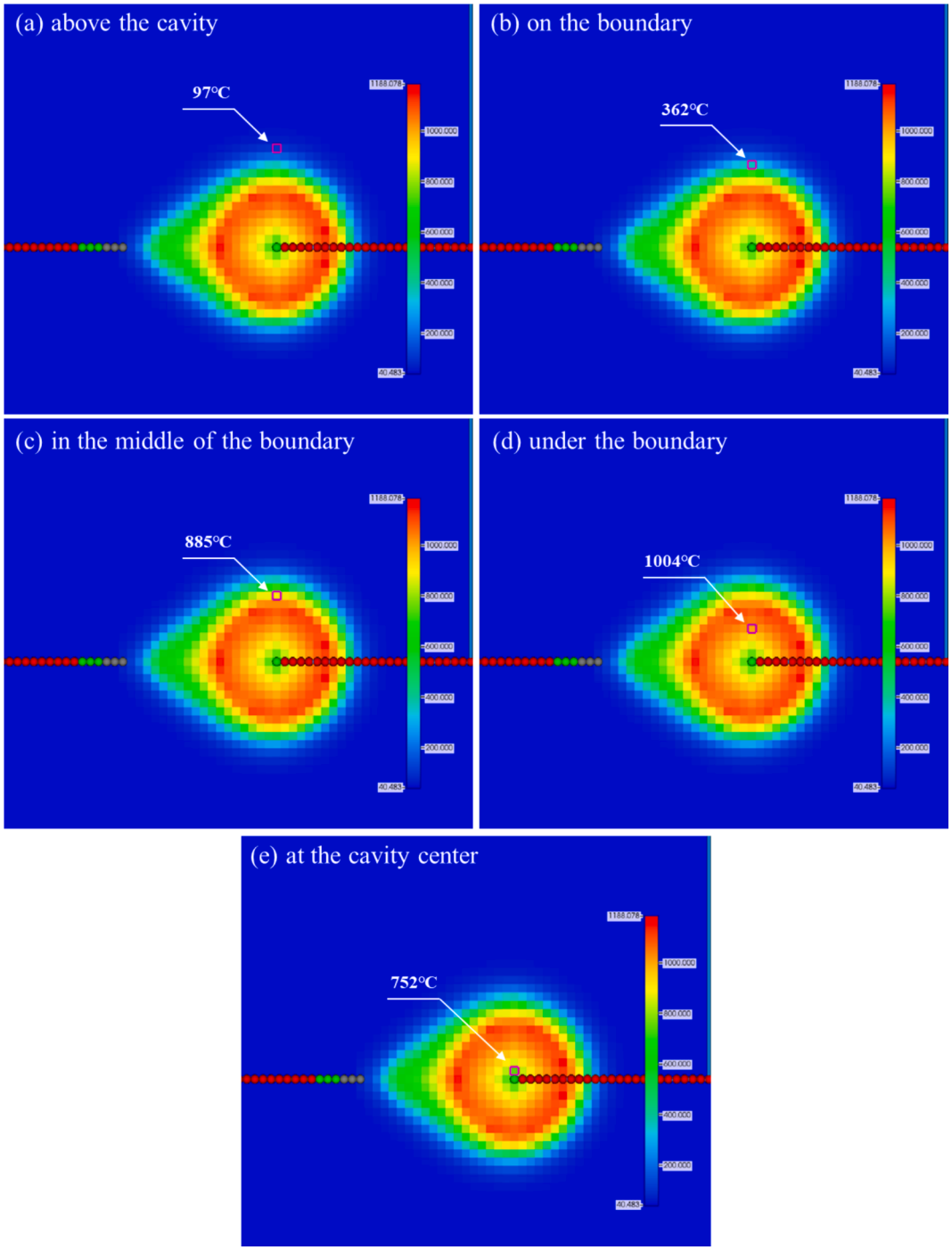

Fig. 11. Temperature of the injection points at the start of water injection.

inclusion of the optimal single-point injection case and the base case. The results confirm that the injection of water outside the cavity seems irrelevant to hydrogen production, which is consistent with the single-point findings. It is also reinforced that water injection under the boundary was the optimal position for hydrogen production, although the difference between scenarios (b) and (c) was less noticeable. However, a comparison between the single-point and multipoint injections illustrates that 11 % more H_2 was yielded in the multipoint scheme. This improved performance revealed that injecting water in a wider range had a positive role in the reactions leading to a higher H_2 yield.

4.2. *Retractable water injection*

Owing to proximity to both the hot char layer and the gas-abundant void, injection of water just below the char boundary exhibited the optimal performance among all the tested scenarios. In addition, it is revealed that multipoint water injection helped further hydrogen production by another 11 %. As illustrated in Figs. 9 and 10, nevertheless, the growing nature of the underground char boundary rendered the optimal injection location less desirable over time and the hydrogen production rate started to decline. To mitigate this trend and obtain a continuous high-rate production of H_2, a technique of retractable water injection points was herein proposed as sketched in Fig. 3. The underlying idea is that upon detecting a decline in the H_2 rate an retraction

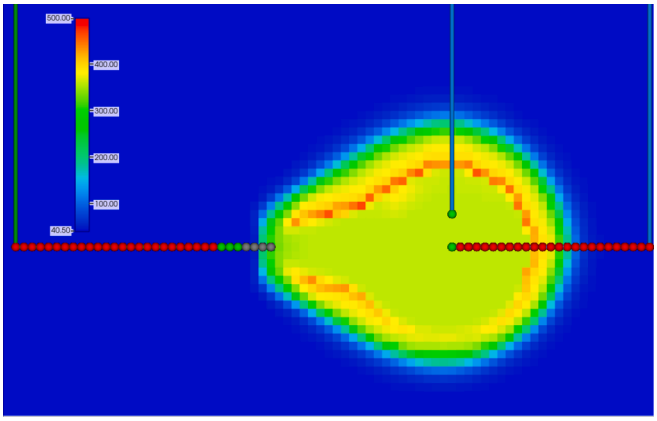

Fig. 12. Temperature profile of the cavity on day 5 for scenario (d).

maneuver of the water injection is performed to align the injection points with the current char boundary such that gasification reactions with water revitalize.

To verify the feasibility to sustain a high H_2 rate with retractable water injection, the post-water injection time of the multipoint under-the-boundary model was extended to 20 days from 5 days. In view of the H_2 rate commencing to decline, a comparative model was created in which the water injection well was retracted 3 grids upward on day 5.

4.2.1. *Effect on hydrogen enhancement*

Fig. 15 compiles the hydrogen production rates for the post water injection period, i.e., 20 days. Gas rates were identical until day 5 when injection points were retracted upwards. The H_2 rate climbed up instantly with water injection and peaked on day 2 at around 10,500 m^3/day, followed by a steady decline as shown in Fig. 15. In the regular scenario, the H_2 rate stabilized after 10 days at approximately 2,300 m^3/day, nearly one fifth of the peak.

The benefits of well retraction were indistinguishable until 1 day later. The plots exhibited that the decline in the H_2 rate was turned around on day 6 upon retraction whereas it persisted in the regular scheme. At the more suitable injection positions, the H_2 rate steadily increased until it entered a relatively plateau state, where the average H_2 rate was close to 10,000 m^3/day as revealed in Fig. 15. In addition, the much longer high-rate period than that of the pre-retraction reflects that water injections helped inhibit cavity growth in the vertical direction, which will be further explained below.

The contribution from retracting water injection points is seen prominent in terms of cumulative hydrogen production, as shown in Fig. 16. Before retraction, a cumulative of 50,000 m^3 H_2 was produced. However, the momentum in hydrogen production slowed down on day 5 in the regular scheme, indicating that more suitable injection points are required. The blue curve demonstrates that the momentum was regained after retracting upward the water injector. At the end of the simulation, a cumulative of nearly 178,000 m^3 H_2 was generated, up from 88,700 m^3 in the non-retraction scenario, showcasing a huge benefit from the technique of retractable water injection.

4.2.2. *Cavity control*

One of the overarching environmental concerns pertaining to UCG derives from the intractable growth of an underground cavity. For example, an unsuccessful cavity growth includes a preferential expansion into the overburden rocks and causes hazardous components to be leached into the overhead aquifers. Furthermore, a high-temperature front incurs thermal stress and fractures in coal and surrounding strata

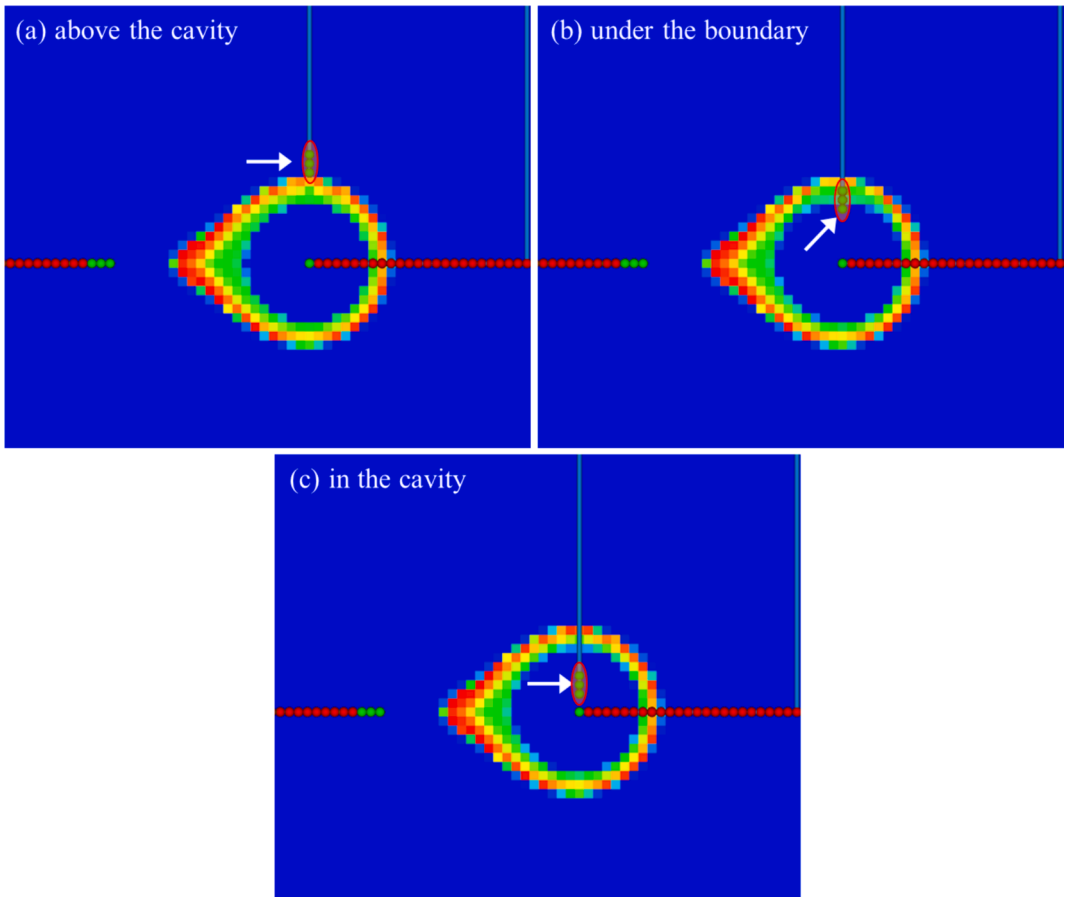

Fig. 13. Locations of various multipoint injection schemes.

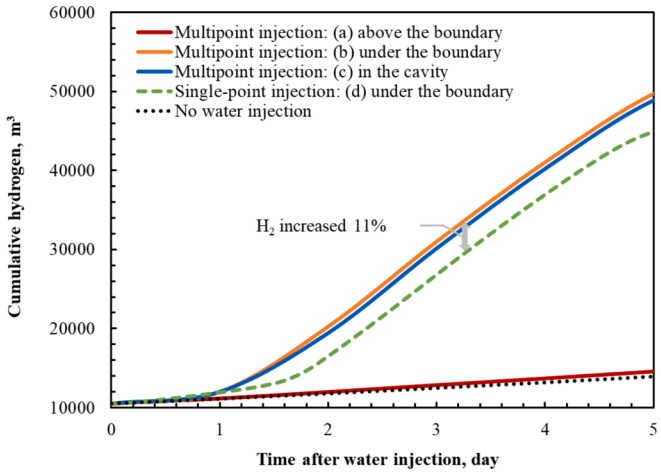

Fig. 14. Comparison of cumulative hydrogen production of multipoint injection scenarios.

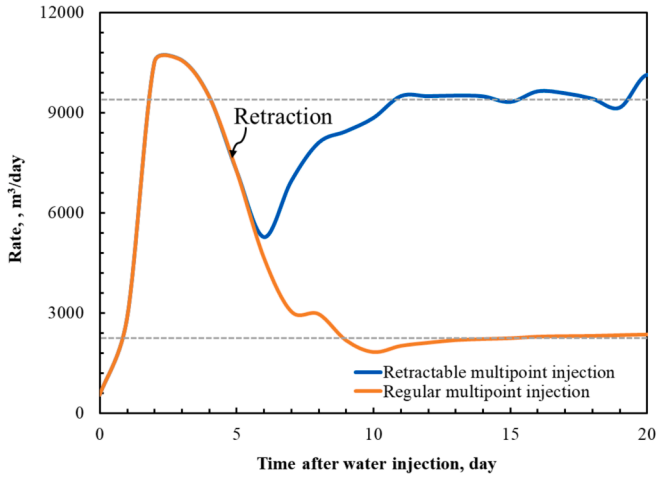

Fig. 15. Hydrogen rate with retractable water injection technique.

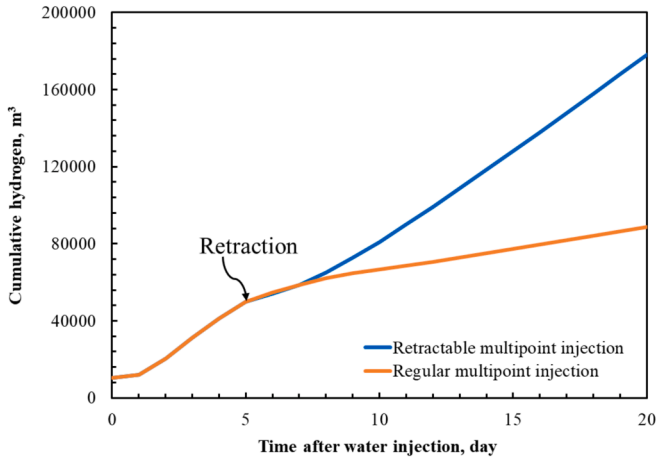

Fig. 16. Cumulative hydrogen production with retractable water injection technique.

and leads to adverse enhanced mass transfer into caprock. The simulation results in this work indicate that water injection helps mitigate this environmental concern through lowering the temperature of the thermal front and thus inhibiting the vertical growth of the UCG cavity.

Fig. 17 shows the temperature of the thermal front for the retractable multipoint water injection technique on day 50, i.e., after 20 days of water injection. Compared to the no water injection process, it manifests that the average front temperature was brought down from 800 ℃ to about 300 ℃. In general, the prevailing temperature in the cavity and boundary was notably dampened by water-assisted endothermic gasification reactions, which, in turn, leads to fewer induced fractures at the thermal front. Fig. 18 presents the cavities in various scenarios in the form of porosity. The original coal porosity is 0.04, and the coal/char entirely consumed void porosity is 0.66 based on the model setting because ash is modelled to stay in situ. Owing to a homogenous coal model, the no water injection UCG model exhibited a more well-rounded cavity with a thick char boundary as indicated in Fig. 18 (a). In contrast, Fig. 18 (b) and (c) show that the water injection process resulted in a much thinner char boundary probably because of a lower-temperature cavity. In the vertical direction, the suppression of water on cavity growth is evident. For example, for the same grid examined in Fig. 18, it was almost a void in the base case (minor char left) while it just started to gasify in the water injection cases. In addition, it further shows that the retractable process played an additional role in limiting the vertical growth of the cavity as the grid porosity had the lowest value in Fig. 18 (c), namely 0.06.

However, the effects on the horizontal cavity growth differed. It seems that an impediment to the vertical direction forced the cavity to grow horizontally. It reveals that the void (red region) in Fig. 18 (b) and (c) exhibited a more evident 'beak' than that in Fig. 18 (a). In particular, Fig. 18 (c) demonstrates that the retractable water injection technique contributed to a longer 'beak' than the regular injection strategy, indicating a stronger effect on cavity control in the vertical direction. The utility of retractable water injection on cavity control bears significant meanings. First, less thermally induced fractures and a control of vertical cavity expansion may help eliminate the concern of aquifer contaminations associated with UCG. In addition, the preference to grow a cavity in the horizontal plane results in a higher coal recovery, rather than losing heat to the caprock. Furthermore, with proper maneuver the integrity of the overburden rock can be maintained for subsequent practices of storing CO_2 in post-UCG cavities.

5. Conclusions

This study utilized numerical simulations to investigate the mechanisms of water-assisted hydrogen production in the context of UCG. The findings revealed that water injection into the inner cavity significantly enhanced hydrogen production, achieving a maximum increase of nearly fivefold compared to scenarios without water injection. This enhancement is attributed to the proximity to both the hot char boundary and the gas-abundant void, with the water–gas shift reaction playing a critical role in boosting hydrogen content. Further simulations indicated that multipoint water injection increased the hydrogen production rate by approximately 11 %, suggesting that injecting water over a wider area effectively promotes hydrogen-oriented endothermic gasification reactions. This approach also highlighted the advantage of positioning the water injection just below the char boundary for optimal results.

To address the decline in hydrogen production over time, a retractable water injection technique was introduced. This innovative method demonstrated substantial potential in sustaining high hydrogen production rates over extended periods. The stable hydrogen rate increased from 2,300 m^3/day to approximately 10,000 m^3/day through the retraction maneuver. Moreover, water injection proved effective in limiting vertical cavity growth, with retractable water injectors having an even more pronounced impact. By carefully maneuvering the retraction of water injection points, the integrity of the overburden rock can be preserved, mitigating the environmental concerns of aquifer contamination. This approach also facilitates the subsequent practice of

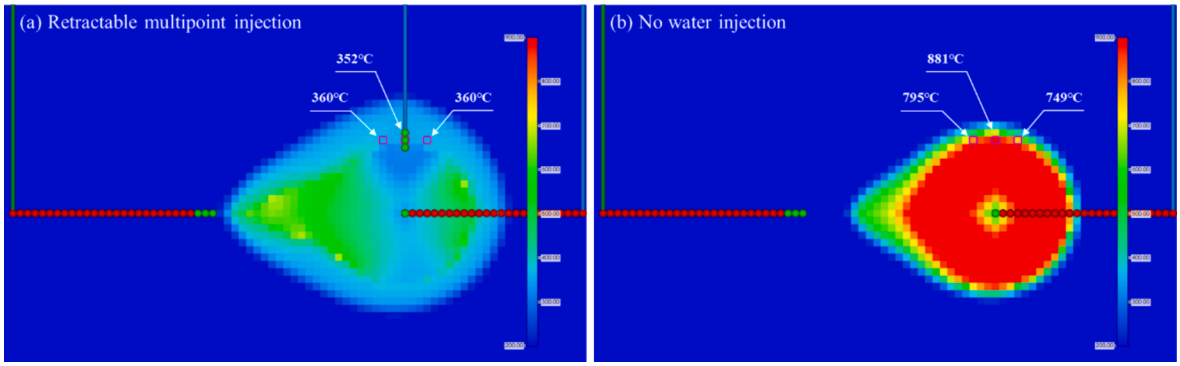

Fig. 17. Cavity temperature comparison after water injection.

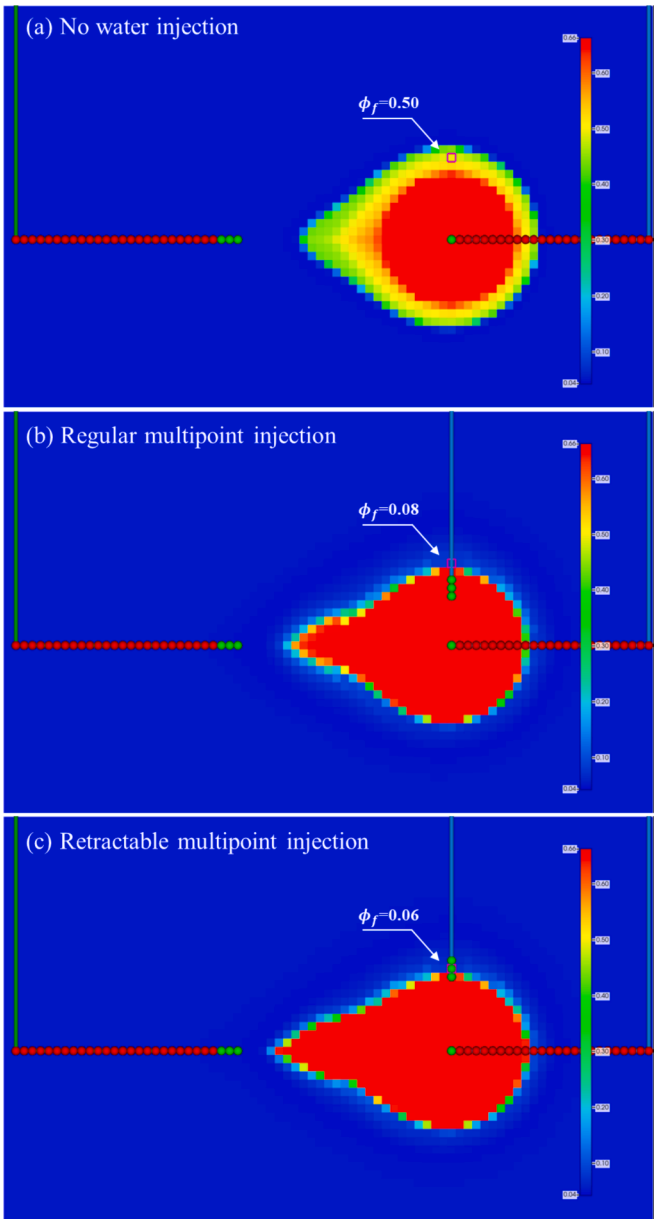

Fig. 18. Cavity growth comparison in porosity after water injection.

storing CO_2 in post-UCG cavities, aligning with environmental protection goals.

The findings highlight UCG's potential as a low-carbon energy source and its crucial role in the hydrogen economy, offering valuable insights for future research. Future studies should focus on optimizing water injection strategies, particularly multi-point injection, to enhance hydrogen yield and reduce energy consumption. Additionally, further investigation into the water–gas shift reaction across different geological and coal rank conditions will improve hydrogen production stability and efficiency, especially in deep or complex coal seams. The scalability of water injection technology has demonstrated significant potential for long-term efficiency improvements, and future research should assess its feasibility in large-scale industrial applications, with a focus on adaptability and regulation across various UCG system sizes. Furthermore, precise control of void expansion during water injection should be explored through real-time monitoring and intelligent feedback systems to ensure environmental safety and prevent groundwater contamination.

CRediT authorship contribution statement

Zixiang Wei: Writing – original draft, Methodology, Data curation, Conceptualization. **Liangliang Jiang:** Writing – review & editing, Supervision, Methodology, Conceptualization. **Aliakbar Hassanpouryouzband:** Methodology, Conceptualization. **Shanshan Chen:** Writing – review & editing. **Yanpeng Chen:** Writing – review & editing, Supervision. **Yiwen Ju:** Methodology, Conceptualization. **Lele Feng:** Writing – review & editing. **Kouqi Liu:** Writing – review & editing. **Jiansheng Zhang:** Writing – review & editing. **Zhangxin Chen:** Writing – review & editing, Supervision, Funding acquisition, Conceptualization. **S.M. Farouq Ali:** Writing – review & editing, Supervision, Methodology.

Declaration of competing interest

The authors declare that they have no known competing financial interests or personal relationships that could have appeared to influence the work reported in this paper.

Acknowledgments

The support of Department of Chemical and Petroleum Engineering, University of Calgary and Reservoir Simulation Group is gratefully acknowledged. This research is partly supported by RIPED, PetroChina, NSERC/Energi Simulation, AITF (iCore), IBM Thomas J. Watson Research Center, and the Energi Simulation/Frank and Sarah Meyer Collaboration Centre for Visualization and Simulation. The research is also enabled in part by support provided by WestGrid and Compute Canada Calcul Canada.

Data availability

Data will be made available on request.

References

[1] Davenport J, Wayth N. 2024 Statistical Review of World Energy. 2024.
[2] Couch G. Underground Coal Gasification; Report No. Contract No: CCC/151IEA n. d.
[3] Xue D, Chen Z, Lu C. Establishment of the comprehensive material balance equation for coalbed methane reservoirs at the gas desorption stage. Fuel 2022; 326. https://doi.org/10.1016/j.fuel.2022.124979.
[4] Mills SJ. Global perspective on the use of low quality coals. IEA Clean Coal Centre 2011;180:1-2. n.d.
[5] Jiang L, Chen Z, Farouq Ali SM. Heavy oil mobilization from underground coal gasification in a contiguous coal seam. Fuel 2019;249:219–32. https://doi.org/10.1016/j.fuel.2019.03.114.
[6] Burton E, Friedmann J, Upadhye R. Best practices in underground coal gasification, vol. 119. Lawrence Livermore National Laboratory; 2006. n.d.
[7] Friedmann SJ. Fire in the hole: underground coal gasification may provide a secure energy supply and reduce greenhouse gas emissions. Lawrence Livermore National Laboratory. Sci Technol Rev 2007. n.d.
[8] Jiang L, Xue D, Wei Z, Chen Z, Mirzayev M, Chen Y, et al. Coal decarbonization: a state-of-the-art review of enhanced hydrogen production in underground coal gasification. Energy Rev 2022;1. https://doi.org/10.1016/j.enrev.2022.100004.
[9] Mao F. Underground coal gasification (UCG): a new trend of supply-side economics of fossil fuels. Nat Gas Ind B 2016;3:312–22. https://doi.org/10.1016/j.ngib.2016.12.007.
[10] Liang J, Yu L. Theory and practice of generating hydrogen by underground pneumatolysis of coal. Sci Technol Rev 1995;13:50–2.
[11] Yang L, Liang J, Yin X. Theory and practice of underground coal gasification to hydrogen technology. Coal Sci Technol 2000;28:37–9.
[12] Jia Z, She X. The mechanism of hydrogen output from underground gasification coal. Energy Technol Manag 2004:37–8.
[13] Fair JC, Larson A, Hasiba HH. AN EVALUATION OF IN SITU COAL GASIFICATIONi. vol. I. Pergamon Press; 1976.
[14] Jiang L, Chen Z, Farouq Ali SM. Feasibility of carbon dioxide storage in post-burn underground coal gasification cavities. Appl Energy 2019;252. https://doi.org/10.1016/j.apenergy.2019.113479.
[15] Yang LH, Zhang X, Zhu K. Hydrogen production in underground coal gasification (UCG). Energy Sources Part A: Recovery Util Environ Eff 2016;38:376–83. https://doi.org/10.1080/15567036.2013.770106.
[16] Jiang L, Chen Z, Farouq Ali SM, Zhang J, Chen Y, Chen S. Storing carbon dioxide in deep unmineable coal seams for centuries following underground coal gasification. J Clean Prod 2022;378. https://doi.org/10.1016/j.jclepro.2022.134565.
[17] Hassanpouryouzband A, Wilkinson M, Haszeldine RS. Hydrogen energy futures - foraging or farming? Chem Soc Rev 2024;53:2258–63. https://doi.org/10.1039/d3cs00723e.
[18] Tarhan C, Çil MA. A study on hydrogen, the clean energy of the future: hydrogen storage methods. J Energy Storage 2021;40. https://doi.org/10.1016/j.est.2021.102676.
[19] Filippov SP, Yaroslavtsev AB. Hydrogen energy: development prospects and materials. Russ Chem Rev 2021;90:627–43. https://doi.org/10.1070/rcr5014.
[20] Linstrom, Peter (2021). NIST Chemistry WebBook. NIST Standard Reference Database Number 69. NIST Office of Data and Informatics. doi:10.18434/T4D303. n.d.
[21] Liang J, Guo L. Review of catalytic gasification of coal for hydrogen production. Proceedings of the 2003 Annual Academic Conference of the Chinese Solar Energy Society, 2003.
[22] Jiang L, Chen Z, Farouq Ali SM. General hydro-geological impact of cleats on underground coal gasification. Fuel 2018;224:128–37. https://doi.org/10.1016/j.fuel.2018.03.037.
[23] Liu S, Zhang J, Liang J, Yu L. Outlook on comprehensive utilization of underground coal gasification. Coal Sci Technol 2003;31:50–3.
[24] Yang L, Zhang X, Liu S, Yu L, Zhang W. Field test of large-scale hydrogen manufacturing from underground coal gasification (UCG). Int J Hydrogen Energy 2008;33:1275–85. https://doi.org/10.1016/j.ijhydene.2007.12.055.
[25] Yin Z, Xu H, Chen Y, Zhao T, Wu J. Experimental simulate on hydrogen production of different coals in underground coal gasification. Int J Hydrogen Energy 2022. https://doi.org/10.1016/j.ijhydene.2022.03.205.
[26] Feng L, Dong M, Qin B, Pang J, Babaee S. H2 production enhancement in underground coal gasification with steam addition: Effect of injection conditions. Energy 2024;291. https://doi.org/10.1016/j.energy.2024.130379.
[27] Stańczyk K, Smoliński A, Kapusta K, Wiatowski M, Świdrowski J, Kotyrba A, et al. Dynamic experimental simulation of hydrogen oriented underground gasification of lignite. Fuel 2010;89:3307–14. https://doi.org/10.1016/j.fuel.2010.03.004.
[28] Stańczyk K, Kapusta K, Wiatowski M, Świdrowski J, Smoliński A, Rogut J, et al. Experimental simulation of hard coal underground gasification for hydrogen production. Fuel 2012;91:40–50. https://doi.org/10.1016/j.fuel.2011.08.024.
[29] Kapusta K, Wiatowski M, Stańczyk K. An experimental ex-situ study of the suitability of a high moisture ortho-lignite for underground coal gasification (UCG) process. Fuel 2016;179:150–5. https://doi.org/10.1016/j.fuel.2016.03.093.
[30] Wiatowski M, Stańczyk K, Świadrowski J, Kapusta K, Cybulski K, Krause E, et al. Semi-technical underground coal gasification (UCG) using the shaft method in experimental mine "barbara. Fuel 2012;99:170–9. https://doi.org/10.1016/j.fuel.2012.04.017.
[31] Seifi M, Abedi J, Chen Z. Application of porous medium approach to simulate UCG process. Fuel 2014;116:191–200. https://doi.org/10.1016/j.fuel.2013.07.091.
[32] Jiang L, Chen Z, Ali SMF. Modelling of reverse combustion linking in underground coal gasification. Fuel 2017;207:302–11. https://doi.org/10.1016/j.fuel.2017.06.097.
[33] Jiang L, Feng L, Gao W, Sun J, Shen A, Liu J, et al. Modelling underground coal gasification: what to start with. Nat Gas Ind B 2023;10:626–37. https://doi.org/10.1016/j.ngib.2023.11.006.
[34] Nourozieh H, Kariznovi M, Chen Z, Abedi J. Simulation study of underground coal gasification in Alberta reservoirs: geological structure and process modeling. Energy Fuel 2010;24:3540–50. https://doi.org/10.1021/ef9013828.
[35] Seifi M, Chen Z, Abedi J. Numerical simulation of underground coal gasification using the CRIP method. Can J Chem Eng 2011;89:1528–35. https://doi.org/10.1002/cjce.20496.
[36] Jiang L, Chen Z, Farouq Ali SM. Thermal-hydro-chemical-mechanical alteration of coal pores in underground coal gasification. Fuel 2020;262. https://doi.org/10.1016/j.fuel.2019.116543.
[37] Computational methods for multiphase flows in porous media. Society for Industrial and Applied Mathematics. n.d.
[38] Britten, J. A., & Thorsness, C. B. (1985). Modeling thermal and material interactions between a reacting char bed and a gasifying/spalling coal proof (No. UCRL-92488; CONF-8508101-3). Lawrence Livermore National Lab., CA (USA). n. d.
[39] Kuyper RA, Van Der Meer TH, Hoogendoorn CJ. TURBULENT NATURAL CONVECTION FLOW DUE TO COMBINED BUOYANCY FORCES DURING UNDERGROUND GASIFICATION OF THIN COAL LAYERS. 1994.
[40] 81. Kuyper, R. A. (1994). Transport phenomena in underground coal gasification channels (transportverschijnselen in ondergrondse kolenvergassingskanalen). Doctoral thesis. n.d.
[41] Van Der Eyden JT, Van Der Meert TH, Hanjalic K, Biezen E, Bruining J. Double-diffusive natural convection in trapezoidal enclosures. vol. 41. 1998.
[42] Deng Q, Yang X, Zhang J. Study on a new correlation between diffusion coefficient and temperature in porous building materials. Atmos Environ 2009;43:2080–3. https://doi.org/10.1016/j.atmosenv.2008.12.052.
[43] Jiang L, Chen S, Chen Y, Chen Z, Sun F, Dong X, et al. Underground coal gasification modelling in deep coal seams and its implications to carbon storage in a climate-conscious world. Fuel 2023;332. https://doi.org/10.1016/j.fuel.2022.126016.
[44] Liu H, Chen F, Pan X, Yao K, Liu S. Method of oxygen-enriched two-stage underground coal gasification. Min Sci Technol 2011;21:191–6. https://doi.org/10.1016/j.mstc.2011.02.018.